

# LES of the LS89 cascade: influence of inflow turbulence on the flow predictions

*L.M. Segui and L.Y.M. Gicquel and F. Duchaine and J. de Laborderie*

CERFACS, Toulouse, France, segui@cerfacs.fr

## ABSTRACT

Free-stream turbulence preceding high-pressure turbine blades has a crucial impact on blade fields including the heat transfer on the wall. Many parameters characterize this turbulence; its intensity, length scales and physical spectrum are addressed in the study of various operating points of the LS89 configuration. Usually, operating points where weak turbulence is injected are well predicted for all fields by Direct Numerical Simulations (DNS) and Large Eddy Simulations (LES). The MUR235 operating point however, with an experimentally injected turbulence level of 6%, remains incorrectly predicted when imposing the experimental values in the simulations. Such difficulties raise many questions amongst which mesh size and turbulent kinetic energy spectrum are of specific importance for LES. Going away from synthetic turbulence injection by imposing a physical energy spectrum can help improving the prediction of heat transfer. From the present study, it seems that turbulent spots developing in a pre-transition region for higher levels of turbulence on the suction side are important features to capture for proper predictions. In parallel, typical structures of boundary layers such as streamwise oriented vortices have been observed and their existence conditions the heat transfer field on the blade wall. From this specific study, all of these physical processes are seen to be highly dependent on the turbulent specification and turbulent transition observed for the MUR235 case. Depending on these inflow specifications, a transitional boundary layer may be encountered upstream of the shock thus modifying the heat transfer profile.

## NOMENCLATURE

HIT	Homogeneous Isotropic Turbulence
LES	Large Eddy Simulation
PSD	Power Spectral Density
TKE	Turbulent kinetic energy
c	Chord
h	Heat transfer coefficient ( $W/(m^2 s)$ )
$q_n$	Heat transfer
s	Curvilinear abscissa around blade
u,v,w	Velocity perturbations
P	Pressure
T	Temperature
$y^+, x^+, z^+$	Wall-distance units for normal and tangential directions
,0	Total
,1	Inlet
,2	Outlet
,w	Wall values

## INTRODUCTION

First stages of high-pressure turbines have undergone an optimization process during the last decades. As a result, the temperature these first stages have to withstand today limits their lifetime as well as the number of cycles before the section of the engine must undergo a revision. In this context, improvement will only come from an indepth understanding of the flow features at the source of the blade heat transfer distribution tools. Flow prediction is a key element in such problems and today LES seems the most promising CFD approach with the potential of providing better insight into the flow and so, is expected to produce accurate average flow solutions around a blade. To gauge such tools, the LS89 turbine blade cascade has recently focused a lot of attention from the LES community, as it is a realistic turbine blade linear cascade configuration studied at VKI by Arts et al. (1990). It represents an excellent test case with a comprehensive database for comparison and has proven to be very sensitive to the turbulence injected; i.e. both the integral length scale and the turbulent intensity are of importance as shown in Gourdain et al. (2010). Certain operating points from the database have been more thoroughly studied due to the difficulty to correctly predict certain fields such as the heat transfer when high Reynolds numbers are encountered. On the suction side for example, it is necessary to correctly predict the boundary layer transition to capture the interactions between the streaky structures generated in the boundary layer and the thermal boundary layer, critical for the correct estimation of the heat transfer in that specific region of the blade. However, the lack of information concerning the integral length scale in Arts et al. (1990) has been tackled in many ways. Some have used a range of values as Gourdain et al. (2010), others have estimated it from available data and presumed features as in Jee et al. (2016). Pichler et al. (2016) have even simulated the grid located ahead of the cascade in the experiments to obtain the length scale value and characterize the turbulence to use. While the latter was ruled out due to cost, the values used in this paper have been taken from the literature. Overall, an extensive range of simulations has been performed to test various effects such as the influence of a higher intensity level and the different physics that might be encountered in this test case. Here, specific issues related to the turbulence injection process are addressed by use of a reference refined mesh LES that is used to analyze the possible loss of information on this specific difficulty whenever using alternative approaches and coarsened meshes.

In the following one describes the configuration and operating points simulated followed by the numerical parameters used for the simulations. A short summary concerning the main problems in injection methods is described and the methodology to be used is detailed. A test case is then presented as validation and illustrations of the consequence of such hypotheses or models. Finally, the results concerning the LS89 case are divided into three subsections. The first subsection shows some reference results using classical synthetic turbulence injection methods with the reference parameters from Arts et al. (1990). The second part investigates the effect on the heat transfer coefficient of spectrum and turbulent intensity at the inlet. Finally, mesh refinement shows differences induced in the wake and how this affects the physics around the vane.

## CONFIGURATION AND OPERATING POINTS

The configuration and computational domain used is represented in Fig. 1. It corresponds to the 2D-profile presented in Arts et al. (1990). The experimental conditions of interest are shown in Table 1. Note that the geometrical description of the blade presents large local oscillations and is not adapted for numerical simulations as shown in Wheeler et al. (2015). To avoid such

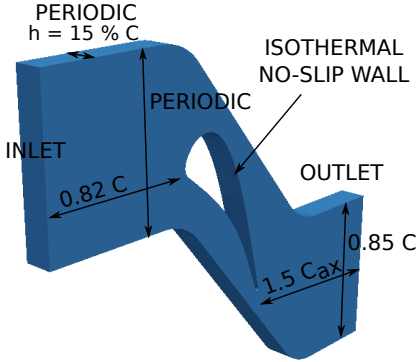


Figure 1: **Control volume.**

	MUR235	MUR129
$P_{01}$ (bar)	1.828	1.849
$T_{01}$ (K)	413.3	409.2
$P_{s2}/P_{01}$	0.57	0.63
$T_w$	301.15	297.75
Mach number at outlet	0.927	0.84
Reynolds outlet	$1.25 \cdot 10^6$	$1.1352 \cdot 10^6$
Inlet turbulent intensity (%)	6	1

Table 1: **Operation point conditions.**

pitfalls, a geometry that keeps coordinate differences under manufacturing tolerance improves the curvature profile and is used in this paper. Inlet domain size is constrained by the development region required for the turbulence to establish a physical spectrum. The outlet region is large enough for the wake to develop and for acoustic waves to exit the domain with no reflection without impacting the upstream flow. This non-reflecting boundary condition imposes the static pressure at the exit as well as a damping coefficient which takes into account the transverse terms as described in Granet et al. (2010). The blade behaves as a non-cooled isothermal surface. This specific computational domain is chosen considering that most of the previous numerical studies rely only on such a pitchwise extent plus the fact that the measurements have only been taken on the central blade of the cascade. Note that a periodicity condition is enforced in the pitchwise direction. The spanwise direction is also taken to be periodic, neglecting then the effect the wall might induce on the blade. The domain limit in this direction is determined by the integral length scale used for the turbulence injection, taking into account its natural growth up to the blade leading edge. This specific hypothesis is under question but outside the scope of this specific work. For this case, a 10 mm domain extent which corresponds to  $15\%C$ , is used and the integral length scale targeted an inflow value of 3.2 mm. Inlet conditions will be described in the following sections.

### Numerical parameters

The code used is the AVBP solver co-developed by CERFACS and IFP-EN, an unstructured cell-vertex based compressible solver, thoroughly tested by Gicquel et al. (2011). It is capable of handling hybrid meshes where layers of prisms are used in the near-wall region of the blade. Tetrahedra are used in the rest of the domain. The convective scheme used in this case is a Finite Element high-order scheme (3rd-order in space, 4th order in time), Quartapelle and Selmin (1993). Two meshes are tested for these simulations. A first reference mesh of 60 million elements is refined near the inlet region, in the near-wall region and in the wake to render a 213 million cells mesh. Both grids are shown in Fig. 2. The  $y^+$  corresponding to the two meshes is of approximately 5 and 3 over the whole blade with corresponding  $x^+ = z^+ \approx 6$ , so these are wall-resolved simulations. The sub-grid scale model used is the WALE model described in Nicoud and Ducros (1999). In the current simulation, no shock capturing technique is used.

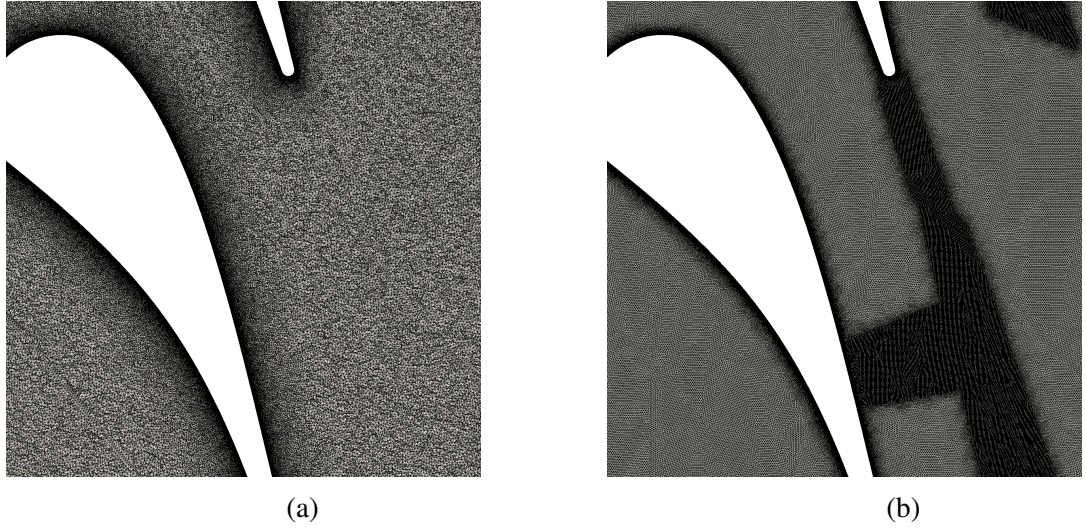


Figure 2: **Mesh details around blade profile for a) 60M and b) 213M cells.**

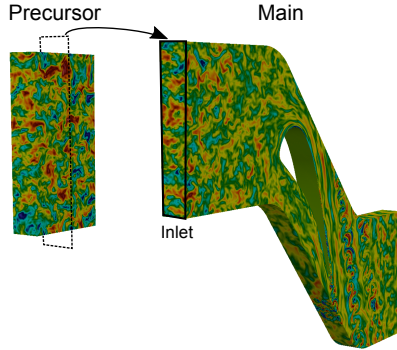


Figure 3: **Global process of the precursor technique; fluctuations extracted from the precursor domain are transferred to the inlet of the main domain.**

## INLET TURBULENCE

Although the integral length scale imposed at the inlet remains an open question, the quality of the turbulence injected is to be accounted for. Indeed, classical synthetic type injection methods, Kraichnan (1970), require some adaptation to develop a physical energy spectrum. Such modeling strategies add onto the difficulty of having an adequate boundary condition implementation and adequate grid resolution as well as numerical schemes. As such, different methods and LES codes will in fact inevitably produce different inflows or turbulent fields prior to the blade. To discriminate the importance of the initial spectrum and move away from synthetic turbulent spectrum that does not give physical solutions, a pre-computed turbulence approach is used to provide information to the boundary conditions. A precursor simulation represented in Fig. 3, performed using the same code, is coupled in this study to the inlet domain to overcome any issue related to the adaptation length underlined previously. For this specific case, only modeling and grid resolution are expected to play a role and can be compared to the synthetic turbulence injection methodology previously mentioned.

An approach that uses an external simulation to provide information to boundary conditions

is not new, Dhamankar et al. (2015). Periodicity simplifies the injection as a HIT field could be imposed without the need for cross-correlations as in wall-bounded flows. As mentioned, the precursor simulation is run simultaneously to the main simulation, which adds a reduced computational cost due to the exchange time required but reduces the amount of memory necessary for the storage.

The turbulent field to be injected into the main domain must be a HIT field as the turbulence injected experimentally is of grid-turbulence type. Computationally, it means that it is necessary to keep the turbulent production in the precursor at the desired level. To do so, the methodology described in Paoli and Shariff (2008) is adopted. It is based on a stochastically forced source term, Eswaran and Pope (1988), applied to the momentum and energy equations and corrected to keep the total energy constant. In terms of boundary conditions specification, the coupling software Open PALM, Duchaine et al. (2015), is then used to send the local velocity perturbation field from the precursor simulation to the inflow domain. Note that this operation is done at each time-step and does not require a coincident mesh. The field extracted from the precursor is interpolated onto the inlet and will serve as the reference fluctuating field. The interpolation performed is of order three to comply with the order of the convective scheme. The precursor field is taken into account in the main domain simulation through characteristic conditions as in Poinsot and Lele (1992). Indeed, directly superimposing the velocities would lead to the reflection of upstream moving waves which would pollute the inlet channel. The wave decomposition takes into account both mean and fluctuating components and a relaxation factor is necessary to ensure the target boundary value. To account for the mean velocity, the Taylor hypothesis is used in this specific application, Taylor (1938), in conjunction with the bulk velocity field of the main simulation. Computationally, this implies that the plane from which the information is extracted in the precursor is not fixed, but moves in the axial direction at the mean bulk velocity of the flow as prescribed by the main domain. Note that such a hypothesis is here relevant since the inlet Mach number is low and fluctuations are of the order of 15% of the mean, Lee et al. (1992).

### Precursor vs. synthetic turbulence

To check the quality of the turbulence injected, a quasi-DNS simulation test case has been performed for a spatially decaying turbulent flow. Spectra and correlations are compared while the applicability of the Taylor hypothesis will be assumed a priori considering a low Mach number at the inlet.

For this test case, the total pressure and temperature are imposed at the inlet of the channel and a turbulent field is injected using the methodology described above. Inlet and outlet characteristic conditions plus periodicity in the pitchwise and spanwise directions are prescribed. Conditions are imposed to have a mean velocity of 100 m/s and a fluctuating velocity of 5 % which corresponds to a Mach number of 0.28. To do this, a channel of  $4 \times 1 \times 1$  mm is simulated for the main domain while the precursor simulation is run using a  $3 \times 1 \times 1$  mm mesh, the turbulent integral length scale being verified to be similar between the precursor and the main domain inlet and corresponding to a value of 0.13 mm.

Figure 4 shows the Q-criterion of the main channel coloured by the norm of the vorticity field for the two cases tested. Two distinct turbulent fields are clearly observed. This is confirmed by the fact that the spectrum quality at the inlet differs and is clearly improved when using the precursor simulation, Fig. 5a. The precursor simulation follows the Kolmogorov tendency up to high wavenumbers, the high limit being associated to twice the characteristic cell

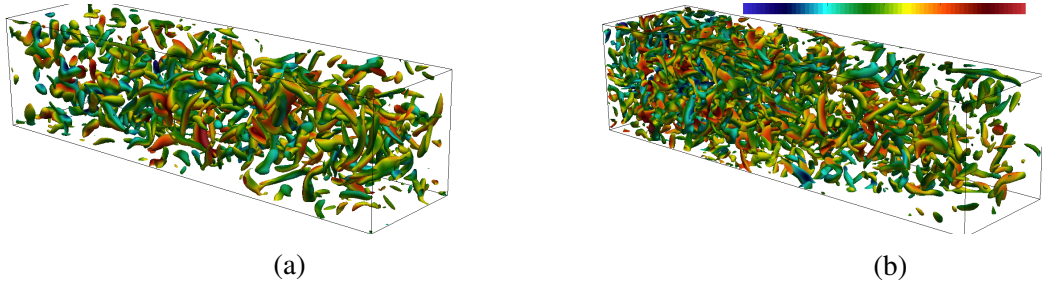
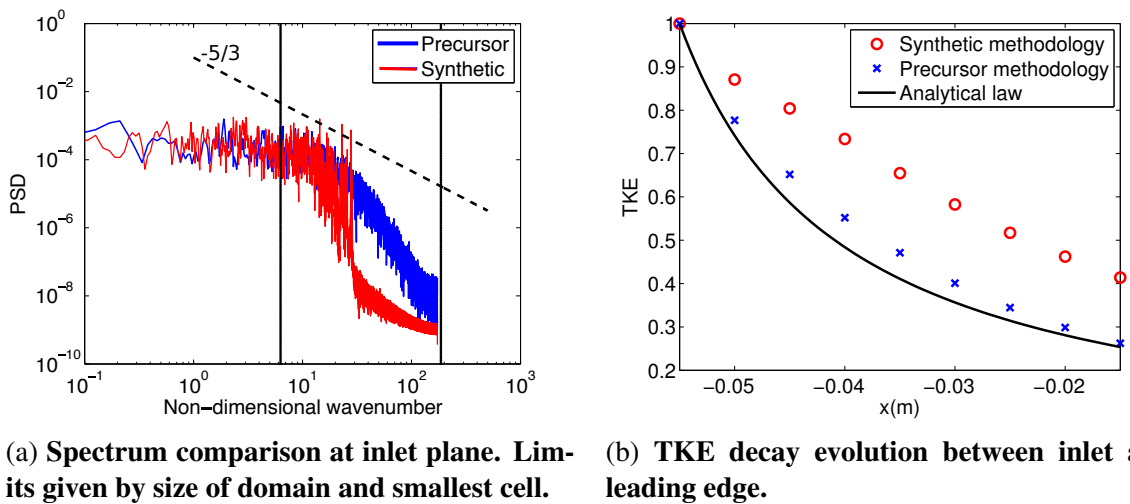


Figure 4: **Q-criterion of channel for a) synthetic b) precursor method coloured by vorticity.**



(a) **Spectrum comparison at inlet plane.** Limits given by size of domain and smallest cell.

(b) **TKE decay evolution between inlet and leading edge.**

Figure 5: **Turbulence injection methods comparison.**

size. The synthetic injection spectrum on the other hand peaks at a lower wavenumber because of the construction method and decays very rapidly indicating that the energy is not properly distributed. Studying Fig. 5b which shows the turbulent kinetic energy decay curve as a function of the axial distance to the channel inlet, it can be observed that the precursor follows quite accurately the analytical evolution of a temporally decaying HIT which it is not the case for the synthetic injection. Note nonetheless that this spatial evolution of the kinetic energy as well as turbulent features will be impacted and only the precursor method provides the proper turbulent flow and a more physical turbulent injection in this case.

Focusing on the precursor method, analyses of the correlations of the axial velocity in the streamwise direction ( $R_{uu}$ ), both spatially and temporally at both inlet and outlet planes for the precursor injection are shown in Fig. 6. Spatial and temporal correlations agree at inlet while they differ slightly on the outlet. Differences are here negligible and most likely induced by boundary condition treatment and implementation. Such results confirm the suitability and physically relevant turbulence at inflow or as it evolves in space. This also justifies the use of the Taylor hypothesis in an otherwise physical reference field, and thus, the application to a more realistic test case.

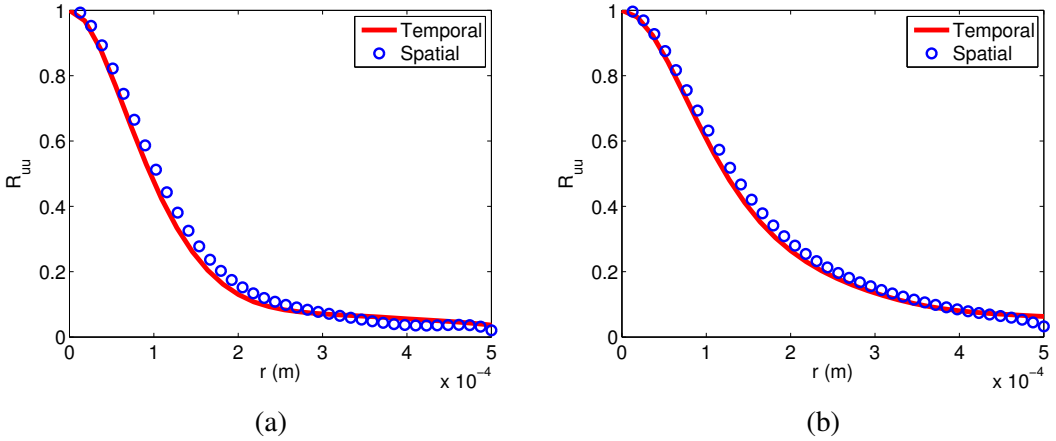


Figure 6: a)  $R_{uu}$  at inlet b)  $R_{uu}$  at outlet.

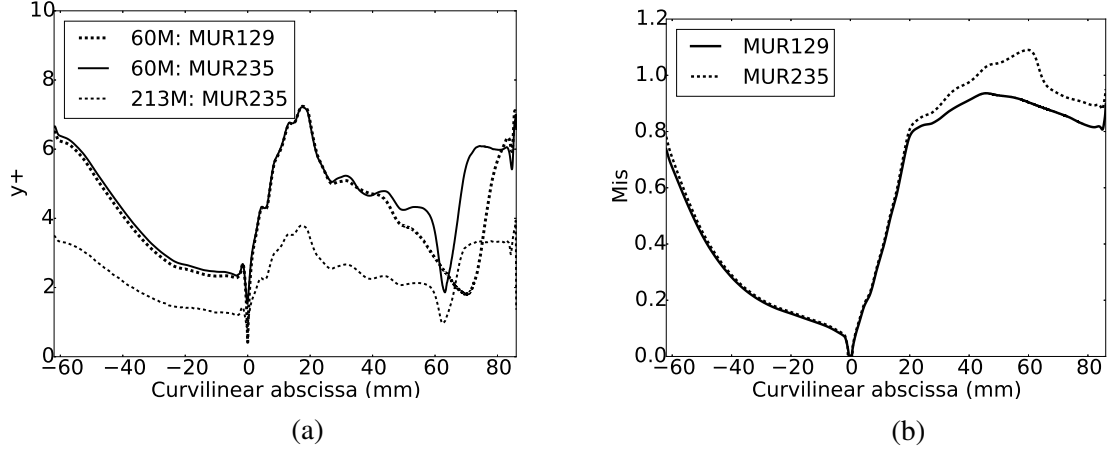


Figure 7: a)  $y^+$  profile around blade b) Isentropic Mach number profile for 60M mesh.

## LS89 RESULTS

The difficulty concerning the operating points with higher free-stream intensity is the incapability of current codes to correctly predict the heat transfer coefficient when comparing it to experimental results. In the following, synthetic turbulence injection predictions are first detailed. These are then compared to the precursor turbulence injection method.

### Synthetic injection: reference results

Simulations of operating points MUR129 and MUR235 are compared to the experimental values on both meshes using the synthetic injection method. The boundary conditions are set to the values indicated in Arts et al. (1990) as noted in Table 1. Profiles of  $y^+$  and the isentropic Mach number are shown in Figs. 7a and 7b to show respectively the refinement level for each mesh and the pressure force distribution around the blade. Note that the values of  $y^+$  on the coarse mesh may be important to adequately capture the blade heat transfer coefficient. Fig. 7b shows the position of the shock wave for the MUR235 case for  $s/c \approx 62$  mm. Figure 8 shows the obtained local flux distribution against experimental data. It can be observed that the heat

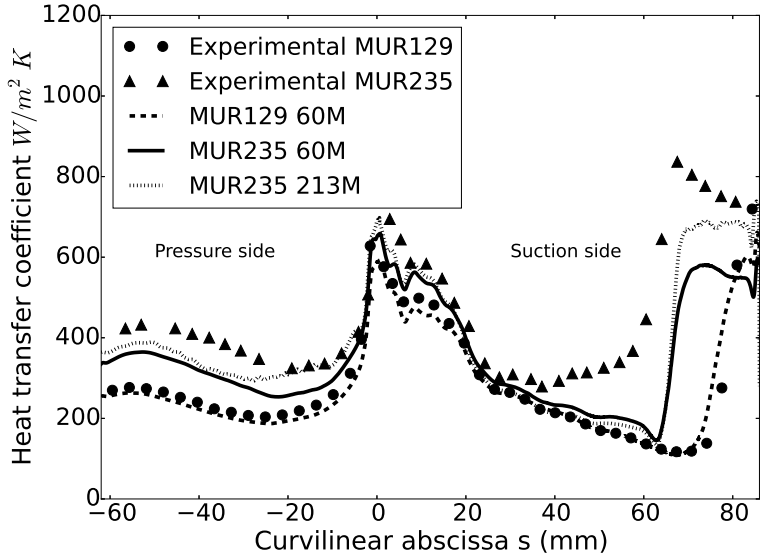


Figure 8: **Heat flux comparison of MUR129 and MUR235 operating points.**

flux coefficient  $h$ , calculated as  $h = \frac{q_n}{T_{0,1} - T_w}$ , is well captured on the whole surface when no turbulence or weak turbulence levels are injected (MUR129) for the coarser mesh.

However, the MUR235 curve is almost at the same level as the MUR129 case for the range  $s \approx 25 - 62$  mm and remains far from the corresponding experimental data. The pressure side however is seen to be notably different between cases although not perfectly captured for the MUR235 case. Only this test case will be retained in the following to gauge its sensitivity to identified modeling parameters. For this specific case, the suction region indeed presents a real challenge as it needs to accurately predict transition, which requires the correct free-stream turbulence, but also the correct capture of the shock position. For both meshes, the shock position seems correctly estimated, the jump after the shock being partly mis-represented. When comparing boundary profiles, not shown, it is seen that the turbulent boundary layer develops more rapidly with turbulence injection. As suggested by Bhaskaran and Lele (2011), the size of the experiment integral length scales is probably larger than the values imposed in the simulation as stated in Fontaneto (2014) and remains to be investigated. This implies that the overall dissipation would be lower and a higher turbulent intensity level should be found on the blade.

### MUR235, effects of 6% vs. 18%, precursor vs. synthetic

In Fig. 9, both the effects of turbulence injection method and inlet turbulence intensity are investigated using the 60 M mesh. It is however difficult to exactly impose the same integral length scales in both methodologies and this leads potentially to uncontrolled discrepancies. Both turbulence injection numerical predictions produce a similar heat transfer coefficient distribution over the whole blade, whatever the value of the injected turbulence intensity. This means that in this case the synthetic turbulence has enough distance for its development to have a physical spectrum. Evaluation of the turbulent intensity prescription on the coarse mesh predictions is also assessed in Fig. 9. Increasing turbulent intensity shows an improved agreement around the leading edge region, complemented with a great improvement on the pressure side

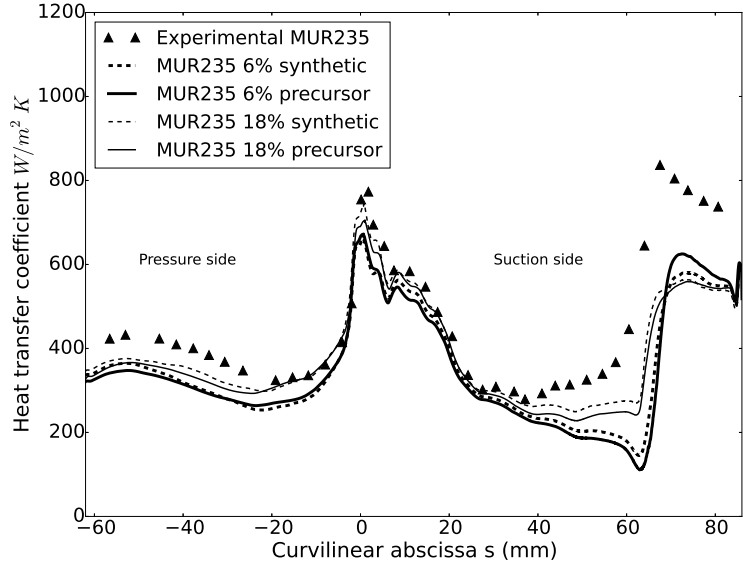


Figure 9: **Heat flux comparison of turbulence injection methods for MUR235 operating point for 60M grid.**

region. The suction side however remains the most challenging. An earlier transition seen when injecting a level of 18% turbulence intensity seems to improve the heat flux prediction, notably near the region of  $s = 25$  mm. When studying instantaneous snapshots at a distance of 0.03 mm normal to the blade surface, temperature contours in the near blade wall flow give an insight to the flow, Fig. 10. The existence of streaks in the buffer layer are observed in all cases when free-stream turbulence is present. This is not the case for the MUR129 operating case where no structure is observed on neither pressure nor suction side. This leads to the conclusion that stretching at the leading edge of the blade and realignment of vortices due to the pressure gradient are responsible for the known spanwise structures characteristic of this region, Wheeler et al. (2015). These specific structures can henceforth be linked to the leading edge heat transfer enhancement. It is furthermore noted that this process is here quite insensitive to the inlet turbulent intensity.

### Grid effect: 60M-213M

In this section, only synthetic turbulence is used with a turbulence intensity level of 18% since similar conclusions apply when using the precursor methodology. In LES, one of the known most important effect relates to the mesh resolution which for the MUR235 case plays a role on the evolution of the turbulence injected at the inlet. Independently of the numerical schemes or the method used to inject turbulence, the increase in the fluctuation intensity intensifies the level of heat transfer. By refining the mesh, the increase in resolution allows smaller structures to arrive to the leading edge as confirmed by Fig. 11 where smaller turbulent structures can be observed when the finer mesh is used.

Aside from the previous effect on turbulence, the most noticeable effect of the grid resolution concerns the acoustic waves emanating from the vortex shedding from the trailing edge

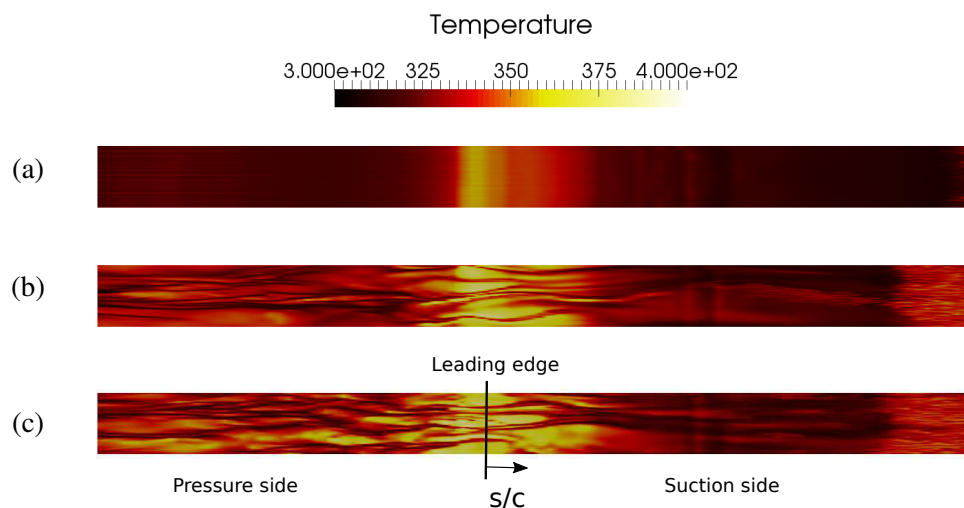


**Figure 10: Instantaneous temperature field at 0.03 mm; i.e. between  $y^+ = 15 - 20$  for a) MUR129, b) MUR235  $u=6\%$ , c) MUR235  $u=18\%$ .**

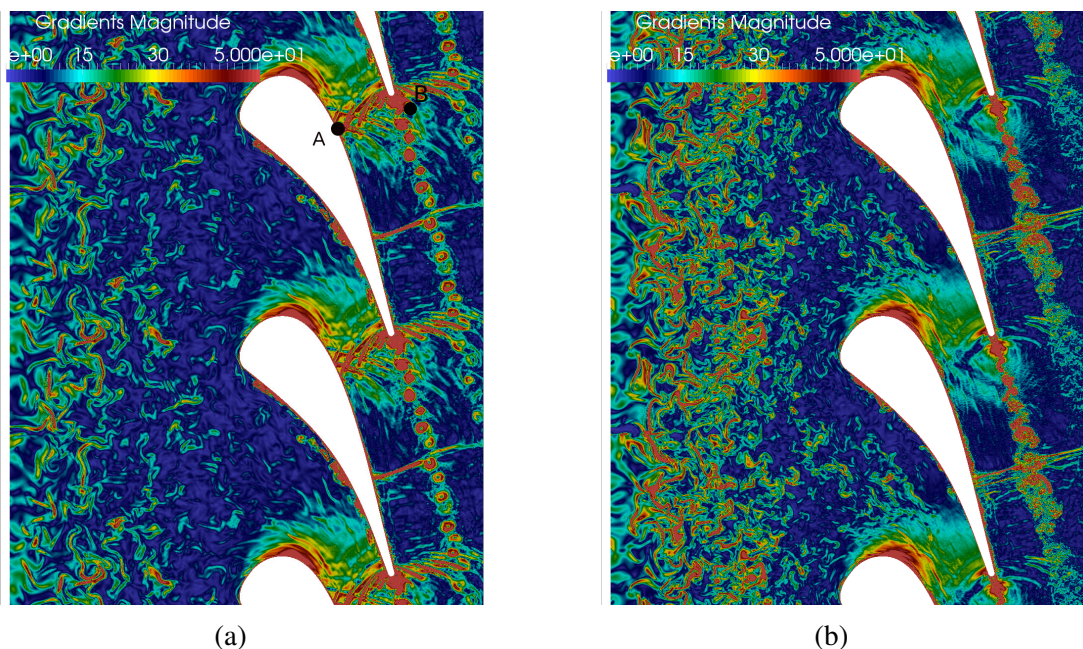


**Figure 11: Density gradient fields for a) 60M and b) 213M cells mesh.**

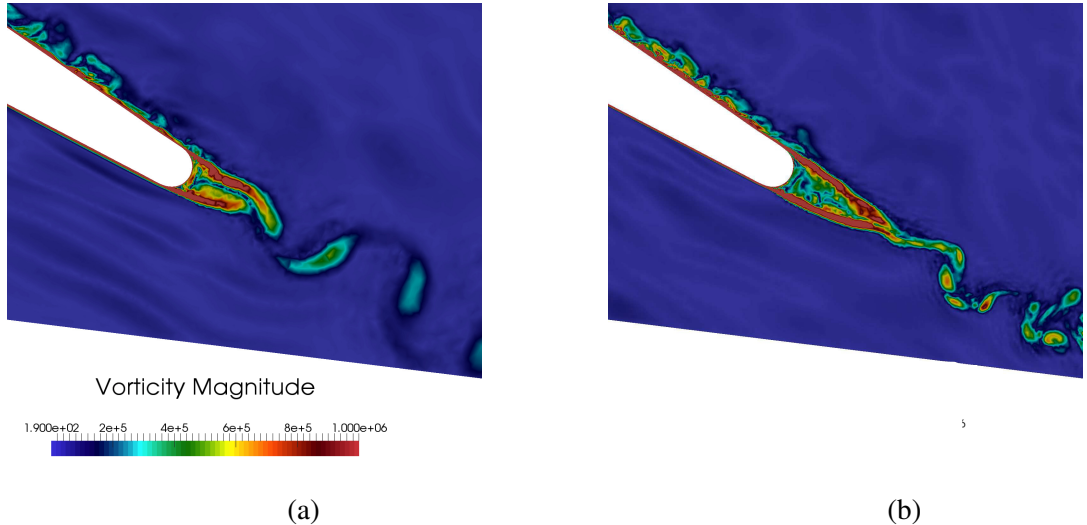


Figure 12: **Blade wakes: instantaneous views of the vorticity magnitude fields for a) the 60M and b) 213M cell meshes.**

seen in Fig. 11. The strong acoustic waves that are then reflected from the blade are much less intense in the refined mesh. Differences may be partly explained by the different refinement in the trailing edge region as seen in Fig. 2, as well as the potential impact of the different turbulent fields in this specific region of the flow. In the coarse case, the flapping characteristic of the vortex shedding is much more intense than for the finer mesh which sheds further downstream as seen in Fig. 12. A similar effect has been shown by Vagnoli et al. (2015), due to a variation of the Mach number.

To further investigate the difference of wave generation between the 60M and 213M grids, local probes named A and B are placed in the wake and on the blade surface of both grids as shown in Fig. 11. Figure 13 represents the pressure spectra recorded by probes A and B for the 60M mesh. Spectrum at probe B clearly highlights a tonal peak that corresponds to the acoustic waves issued from the wake at a frequency of 43kHz and which is the exact same frequency found for probe A on the wall. This confirms the strong influence of the waves created by the vortex shedding on the suction side boundary layer prior to the pre-transition zone. This specific peak is however not clearly visible in the pressure spectrum recorded in the wake at this position on the finer mesh. Together with Fig. 12, this indicates a much less intense vortex shedding than for the 60M grid. As a consequence the spectrum recorded by probe A contains many less tonal frequencies than the coarse grid.

The presence or absence of the waves has however a direct impact on the boundary layer, and thus, on the heat transfer coefficient shown in Fig. 14. Indeed, the boundary layer of the coarse mesh transitions upstream when compared to the fine mesh. The acoustic waves seem to be driving the transition location, where even low-amplitude waves are seen to lead to a pre-transition for the 213M mesh. Figure 14 also shows that the fine mesh predicts more accurately the shock position and the level of  $h$  downstream from the shock if compared to the coarse mesh.

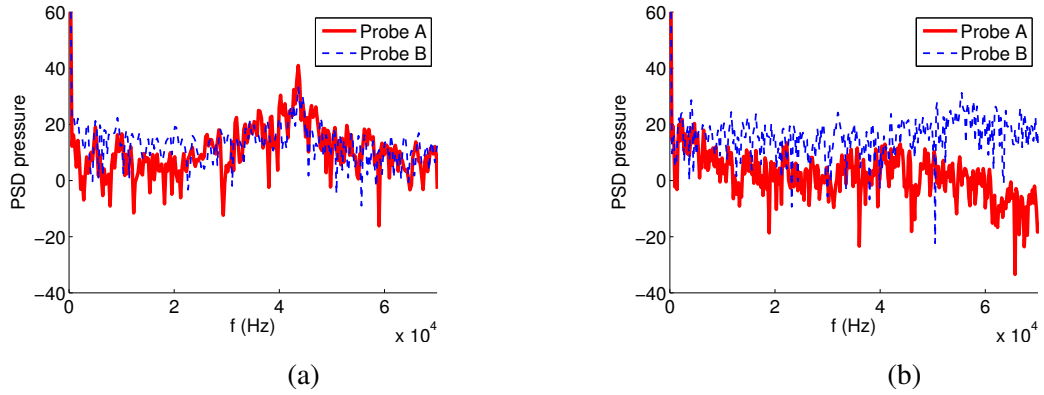


Figure 13: **Spectral content of probes located at various locations for the a) 60M and b) 213M cell meshes.**

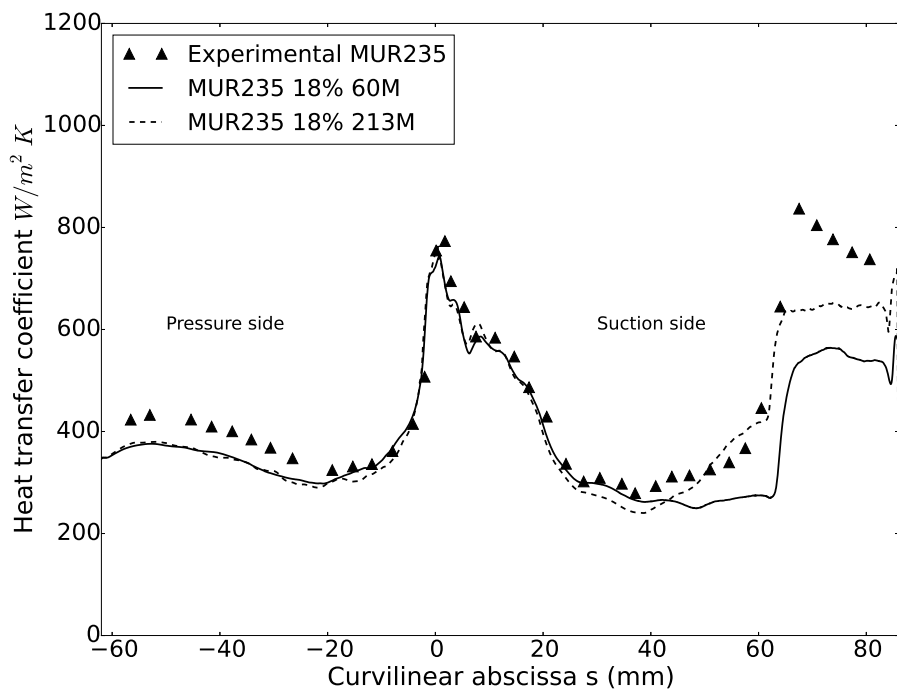


Figure 14: **Heat flux comparison of MUR235 with fine mesh.**

## CONCLUSIONS

An alternative approach to classical synthetic models for turbulence injection has been implemented and validated in a quasi-DNS test case. The spectrum and evolution when comparing synthetic and precursor approaches show the improvement in the physics predicted. When applied to the LS89 case, where the influence of the turbulence injected is known to be critical, both methodologies show no great differences in heat flux predictions. The distance from the boundary to the blade seems sufficient for the turbulence to develop a physical spectrum. The artificial increment of the intensity is found to increase the heat transfer coefficient for the same integral length scale. Mesh refinement shows different behaviour in the boundary layer which affects the wake and the acoustic waves shed that are seen to impact the contiguous vane heat transfer field.

## ACKNOWLEDGEMENTS

This work was granted access to the HPC resources of CINES under the allocation 2016-x20162a6074 made by GENCI. The authors also acknowledge CENAERO for providing the geometry used for this document. This study was also funded by the Marie Curie Actions, European Community's Seventh Framework Programme no. 290042 (COPA-GT).

## REFERENCES

- T. Arts, M. de Rouvrot, Lambert, and A.W. Rutherford. Technical report, Von Karman Institute for Fluid Dynamics, 1990.
- R. Bhaskaran and S.K. Lele. Heat transfer prediction in high pressure turbine cascade with free-stream turbulence using les. In *41st AIAA Fluid Dynamics*, Honolulu, Hawaii, 2011. AIAA 2015-3266.
- N.S. Dhamankar, G.A. Blaisdell, and A.S. Lyrintzis. An overview of turbulent inflow boundary conditions for large eddy simulations. In *22nd AIAA Aviation*, Dallas, 2015. AIAA 2015-3213.
- F. Duchaine, S. Jauré, D. Poitou, E. Quémérais, G. Staffelbach, T. Morel, and L. Gicquel. Analysis of high performance conjugate heat transfer with the openpalm coupler. *Journal of Computational Science and Discovery* 8, 015003, 2015.
- V. Eswaran and S. B. Pope. An examination of forcing in direct numerical simulations of turbulence. *Computers & Fluids*, 16:257–278, 1988.
- F. Fontaneto. *Aero-thermal performance of a film-cooled high pressure turbine blade/vane: a test case for numerical codes validation*. PhD thesis, University of Bergamo, 2014.
- L.Y.M. Gicquel, N. Gourdain, J.-F. Boussuge, H. Deniau, G. Staffelbach, P. Wolf, and T. Poinsot. High performance parallel computing of flows in complex geometries. *Comptes Rendus Mécanique*, 339(2-3):104 – 124, 2011.
- N. Gourdain, F. Duchaine, E. Collado, and L. Gicquel. Advanced numerical simulation dedicated to the prediction of heat transfer in a highly loaded turbine guide vane. In *ASME Turbo expo*, Glasgow, UK, June 2010. GT2010-22793.

- V. Granet, O. Vermorel, T. Léonard, L. Gicquel, and T. Poinsot. Comparison of Nonreflecting Outlet Boundary Conditions for Compressible Solvers on Unstructured Grids. *AIAA Journal*, 48(10):2348–2364, 2010.
- S. Jee, J. Joo, and G. Medic. Large-eddy simulation of a high-pressure turbine vane with inlet turbulence. In *ASME Turbo Expo 2016*, Seoul, South Korea, 2016. GT2016-56980.
- R.H. Kraichnan. Diffusion by a random velocity field. *Phys. Fluids* , 13:22–31, 1970.
- S. Lee, S. Lele, and P. Moin. Simulation of spatially evolving turbulence and the applicability of taylor's hypothesis in compressible flows. *Phys. Fluids A*, 4(7):1521–1530, 1992.
- F. Nicoud and F. Ducros. Subgrid-scale stress modelling based on the square of the velocity gradient. *Flow, Turb. and Combustion* , 62(3):183–200, 1999.
- R. Paoli and K. Shariff. Turbulent condensation of droplets: direct simulation and a stochastic model. *J. Atmos. Sci.* , 2008.
- R. Pichler, J. Kopriva, G. Laskowski, V. Michelassi, and R. Sandberg. Highly resolved les of a linear hpt vane cascade using structured and unstructured codes. In *ASME Turbo Expo 2016*, Seoul, South Korea, 2016. GT2016-57189.
- T. Poinsot and S. Lele. Boundary conditions for direct simulations of compressible viscous flows. *J. Comput. Phys.* , 101(1):104–129, 1992.
- L. Quartapelle and V. Selmin. High-order Taylor-Galerkin methods for non-linear multidimensional problems. *Finite Elements Fluids*, 1993.
- G. I. Taylor. The spectrum of turbulence. *Proc. R. Soc. London Ser. A* 164, 476, 1938.
- S. Vagnoli, T. Verstraete, B. Mateos, and C.H. Sieverding. Prediction of the unsteady turbine trailing edge wake flow characteristics and comparison with experimental data. *Journal of Power and Energy*, 2015.
- A.P.S. Wheeler, R.D. Sandberg, N.D. Sandham, R. Pichler, V. Michelassi, and G. Laskowski. Direct numerical simulations of a high pressure turbine vane. In *ASME Turbo Expo 2015*, Montreal, Canada, 2015. GT2015-43133.